REPORT DOCUMENTATION PAGE

Form Approved
OMB No. 0704-0188

1. AGENCY USE ONLY (Leave blank)	2. REPORT DATE	3. REPORT TYPE AND DATES COVERED
	Nov 90	Final 1 Oct 87 - 30 Sep 90

4. TITLE AND SUBTITLE

Magnetic Quasicrystals

5. FUNDING NUMBERS

DAAL03-87-K-0149

6. AUTHOR(S)

Takeshi Egami

7. PERFORMING ORGANIZATION NAME(S) AND ADDRESS(ES)

Univ of Pennsylvania
Philadelphia, PA 19104

8. PERFORMING ORGANIZATION REPORT NUMBER

9. SPONSORING/MONITORING AGENCY NAME(S) AND ADDRESS(ES)

U. S. Army Research Office
P. O. Box 12211
Research Triangle Park, NC 27709-2211

10. SPONSORING/MONITORING AGENCY REPORT NUMBER

ARO 24008.3-MS

11. SUPPLEMENTARY NOTES

The view, opinions and/or findings contained in this report are those of the author(s) and should not be construed as an official Department of the Army position, policy, or decision, unless so designated by other documentation.

12a. DISTRIBUTION/AVAILABILITY STATEMENT

Approved for public release; distribution unlimited.

12b. DISTRIBUTION CODE

13. ABSTRACT (Maximum 200 words)

The atomic structure of liquid-quenched amorphous $Al_{90}Fe_xCe_{10-x}$ ($x = 5, 7$) was studied by pulsed neutron and x-ray scattering. The atomic pair-density function determined by pulsed neutron diffraction indicates that a significant portion of Al–Fe distances is anomalously short, while some part of the Al–Al distances is anomalously long. Both neutron and x-ray scattering showed the presence of a prepeak in the structure factor. These results suggest that a strong interaction between Al and Fe modifies the structure of this glass, leading to chemical and topological short-range ordering.

14. SUBJECT TERMS

Magnetic Quasicrystals, Metallic Glasses, Alloy Systems, Aluminum Alloys

15. NUMBER OF PAGES

16. PRICE CODE

17. SECURITY CLASSIFICATION OF REPORT	18. SECURITY CLASSIFICATION OF THIS PAGE	19. SECURITY CLASSIFICATION OF ABSTRACT	20. LIMITATION OF ABSTRACT
UNCLASSIFIED	UNCLASSIFIED	UNCLASSIFIED	UL

NSN 7540-01-280-5500

Standard Form 298 (Rev 2-89)
Prescribed by ANSI Std Z39-18
298-102

ARO 24008.3-MS

MAGNETIC QUASICRYSTALS

FINAL REPORT

T. EGAMI

Nov. 30, 1990

U.S. ARMY RESEARCH OFFICE

DAAL03-87-K-0149

UNIVERSITY OF PENNSYLVANIA, PHILADELPHIA, PA 19104-6272

APPROVED FOR PUBLIC RELEASE;

DISTRIBUTION UNLIMITED.

TABLE OF CONTENTS

1. Goal of the Project 3

2. Achievements 4

2-1. Atomic and Magnetic Structure of Quasicrystalline Al-Mn-Ge-Cu 6

2-2. Atomic Structure of Amorphous Al-Fe-Ce 10

3. List of Publications 12

4. List of Participating Scientific Personnel 12

5. References 13

Figure Captions

Figures

Appendix A:

"Atomic Structure of Amorphous $Al_{90}Fe_xCe_{10-x}$", H. -Y. Hsieh, B. H. Toby, T. Egami, Y. He, S. J. Poon and G. J. Shiflet, J. Mater. Res., 5, Dec. (1990).

Appendix B:

"Atomic Short Range Order in Amorphous $Al_{90}Fe_xCe_{10-x}$", H. -Y. Hsieh, T. Egami, Y. He, S. J. Poon and G. J. Shiflet, submitted to J. Non-Cryst. Solids.

1. GOAL OF THE PROJECT.

Most materials are either crystalline or amorphous. Crystalline materials have a periodic atomic structure while amorphous materials are aperiodic. Quasicrystals, on the other hand, have an atomic structure characterized by two or more periodicities which are incommensurate to each other. Thus the structure has long range orientational and positional order, but no translational symmetry. This departure from the requirement of translational symmetry allows the solids to have symmetries not possible for crystals, such as icosahedral symmetry and decagonal symmetry.

New symmetries not allowed for crystals should result in new symmetry related properties so far unobserved for crystals. The property we focussed is magnetism, since the dependence of magnetic properties on the crystalline symmetry is well known. For instance, we have shown that the magnetic anisotropy energy of an icosahedral solid takes the form, to the lowest order,

$$E(\vec{M}) = K_6 \left[Y_6^0 - \left(\frac{7}{11}\right)^{1/2} (Y_6^5 - Y_6^{-5}) \right]$$

$$- \frac{K_6}{16} \left[231\cos^6\theta - 315\cos^4\theta + 105\cos^2\theta - 5 + 42\cos\theta\sin^5\theta\cos 5\phi \right]$$

where Y_l^m are the spherical harmonics of the magnetization direction (θ, φ). Note that the lowest order is the 6-th order, with 4-th and 2nd order missing. Since the magnitude of the anisotropy energy decreases very quickly with the increasing order, the magnetic anisotropy energy of a ferromagnetic icosahedral quasicrystal is much smaller than the cubic crystals which are dominated by the 4-th order terms, and hexagonal, tetragonal or orthorhombic crystals which have large two-fold terms. Thus the icosahedral quasicrystalline ferromagnets should exhibit very small magnetic anisotropy and consequently high magnetic permeability, and may provide some use as a soft magnetic material. The goal of the present project has been to develop such ferromagnetic quasicrystals and study their structure and properties.

2. ACHIEVEMENTS.

At the time we submitted the research proposal of this project no ferromagnetic quasicrystal has been known. Together with Dr. O'Handley of MIT and his colleagues we found an indication that a melt-quenched (rapidly cooled) Co-Er alloy may be a ferromagnetic quasicrystal. Further research, however, has shown that the alloy was merely crystalline, and not quasicrystalline. We made further considerable effort by sputter depositing the Co-Er and Co-Er-Si alloy system, but the results have been negative.

In the meantime two overseas reports claimed an observation of ferromagnetism in quasicrystalline solids. The first was by Chinese researchers on Al-Fe-Ce [1], and the second was from Japan on Al-Ge-Mn and Al-Ge-Mn-Cu [2]. The magnetic moment reported in Al-Fe-Ce was very small, suggesting that it may be due to impurity phases. At the same time amorphous alloys with very high specific tensile strength were produced out of the same alloy system [3,4]. In particular, this system has very high concentrations of aluminum, up to 90 atomic %. Usually amorphous alloys with such a high concentration of the primary element are unstable and cannot be produced by rapid quenching, since they often violate the size rule established by the principal investigator [5]. It was suspected therefore that this unusual glass forming tendency and the formation of a quasicrystal may have something in common, and we decided to carry out the neutron and x-ray study of the atomic structure of amorphous Al-Fe-Ce. As expected we found that Fe strongly modifies the local structure of Al, and results in strong short range ordering, as discussed below.

The other alloy system, Al-Ge-Mn and Al-Ge-Mn-Cu, shows a larger magnetic moment, and apparently is more stable. However, its magnetic moment, σ, is quite small while its Curie temperature, T_c, is relatively high. For instance for $Al_{40}Ge_{25}Mn_{25}Cu_{10}$, σ = 1.5 emu/g and T_c = 467 K. Therefore we conjectured that while it was possible that this magnetism was merely due to a small amount of the second phase, possibly crystalline, such as the grain boundary

phase, representing uninteresting possibility, it was equally possible that the system was actually ferrimagnetic with a sizable local moment, and the smallness of the total moment might be the consequence of partial cancellation. To resolve this question we studied this alloy by neutron scattering. The result shows that the second, more interesting case is true, and we indeed made the first observation of the magnetic scattering from the quasicrystal. The result shows that:

1. Strong magnetic order can exist in quasicrystals.

2. In this particular case the magnetic symmetry is lower than the lattice (f.c.i.) symmetry, suggesting that it is either ferrimagnetic or antiferromagnetic.

3. By changing the antiferromagnetic interaction to a ferromagnetic one, it should be possible to produce strongly magnetic quasicrystals.

2-1. Atomic and Magnetic Structure of Quasicrystalline $Al_{40}Ge_{25}Mn_{25}Cu_{10}$.

The atomic and magnetic structure of quasicrystalline $Al_{40}Ge_{25}Mn_{25}Cu_{10}$ was studied through x-ray and neutron scattering measurements. The melt-spun flake samples were provided by Prof.

Masumoto's group in the Institute for Materials Research, Tohoku University, Sendai, Japan. The x-ray scattering measurements were made using synchrotron radiation at the X-7A beamline of the National Synchrotron Light Source (NSLS) of Brookhaven National Laboratory. The synchrotron radiation was monochromated by a channel-cut Si crystal at 25 keV, and the scattered x-rays were detected by a Ge energy sensitive detector. The pulsed neutron scattering measurements were done at the Special Environment Powder Diffractometer of the Intense Pulsed Neutron Source (IPNS) of Argonne National Laboratory, and magnetic neutron scattering measurements at the reactor of the National Institute for Standard and Technology (NIST).

The indexing of the diffraction peaks shows that there exists an extinction rule, that the six indices are either all even or all odd, similarly to the extinction rule for the face centered cubic (f.c.c.) structure. Therefore, this solid has the face centered icosahedral (f.c.i.) structure, just as quasicrystalline $Al_{65}Cu_{25}Fe_{10}$ [6]. We have shown recently that the structure of $Al_{65}Cu_{25}Fe_{10}$ is given by the projection of the primitive six-dimensional hypercubic lattice with the NaCl type atomic decoration using the projection window inflated by τ compared to the standard window to produce the 3-d Penrose tiling [7]. This conclusion was obtained by comparing the atomic pair distribution function (PDF) determined by the synchrotron x-ray scattering measurement with that calculated for the model, as shown in Fig. 1. This is the first example of the

primitive lattice quasicrystal, since we also found that other quasicrystals, such as Al-Li-Cu or Al-Mn-Si, have a structure projected from the non-primitive, decorated 6-d lattice, with a high density of local phason defects, or the lattice sites unoccupied by atoms. We suggest that the primitive nature of the 6-d lattice is the origin of the absence of phason defects in $Al_{65}Cu_{25}Fe_{10}$. The phason defects are the local deviations from the perfect quasicrystalline structure, and linear phason defects which broaden the diffraction peaks have been observed in all the icosahedral solids except for this solid. The PDF determined for Al-Ge-Mn-Cu indicates that the same structure describes this solid as well, if Al is replaced by random mixture of Al and Ge, Cu replaced by Mn, and Fe by Cu.

Non-spin-polarized neutron scattering experiments were performed at the NIST in Gaithersburg, MD using neutrons with 2.6 Å in wavelength. The powder sample weighing about 50 g was contained in an Al tube, and placed in an Al low temperature furnace. We found that the height of the diffraction peaks change very significantly by annealing. In the same temperature range Tsai et al. [2] found a large exo-thermic peak in the differential scanning calorimetry, and concluded, without other evidences, that it was due to crystallization. However, since the peak positions do not change, we do not think that crystallization is taking place. Instead, what is happening seems to be the increase in the 6-d NaCl type atomic chemical ordering, and the modelling certainly

confirms this.

Most of the measurements were carried out on the sample annealed at 275 C for 30 min. to maximize the ordering. The results showed that the many diffraction peaks depend upon temperature much more than expected from the Debye-Waller factor as shown in Fig. 2. In particular one peak at Q = 2.53 $Å^{-1}$ disappears above 270 K, at the Curie temperature as shown in Fig. 3. Therefore this peak must be a purely magnetic peak. Thus we have for the first time observed the magnetic neutron scattering from a quasicrystal.

The extra peak at 2.53 $Å^{-1}$ can be indexed as (110000), with the quasicrystalline lattice constant of 8.90 Å, thus violating the f.c.i. extinction rule. Therefore the magnetic sublattice must be breaking the f.c.i. symmetry. This suggests that the magnetic order is either antiferromagnetic or ferrimagnetic. While ferromagnetic sublattice is commensurate with the lattice and does not break the lattice symmetry, antiferromagnetic or ferrimagnetic order tends to double the lattice periodicity. We are planning to carry out spin-polarized neutron scattering experiments at the High-Flux Reactor of Brookhaven National Laboratory (under the NSF support) when the reactor resumes operation most likely early next year, to separate the magnetic peaks more clearly from the nuclear peaks and to determine the magnetic structure. It is not clear at this moment whether the system is truly a ferrimagnet, or a

partially frustrated antiferromagnet. In the latter case a perfect quasicrystal would have no magnetic moment, and the moment is due only to the defects. This observation suggests that if by chemical modification the antiferromagnetic exchange interaction could be changed to ferromagnetic interaction there is a good possibility for a strong ferromagnetic quasicrystal.

2.2 Atomic Structure of Amorphous Al-Fe-Ce.

The atomic structure of melt-spun ribbons of $Al_{90}Fe_xCe_{10-x}$ was studied by pulsed neutron and x-ray scattering measurements. The samples were provided by Prof. Poon's group at the University of Virginia. As detailed in two publications on this subject attached as Appendices, the neutron and x-ray scattering measurements clearly showed that the Al-Fe distance in this alloy system is anomalously short compared to the sum of the atomic radii, about 2.5 Å vs. 2.69 Å. This is most likely the consequence of the strong s-d hybridization between Al and Fe. This strong Fe-Al interaction results in strong compositional as well as topological short range ordering around Fe, and Fe has only <u>six</u> close Al neighbors at 2.5 Å and 4 more slightly distant Al neighbors at about 2.8 Å.

Also the ordering among Fe atoms is very far from random. The structure factor of this alloy system has a strong pre-peak at around 1.4 ~ 1.5 $Å^{-1}$, which extrapolates to about 1.6 $Å^{-1}$ for

$Al_{90}Fe_{10}$, while for a random distribution of Fe atoms with a short range ordering due to the repulsion among Fe we expect to have a peak at 1.3 $Å^{-1}$. This peak position is close to that of a quasicrystalline Al-Fe [8], suggesting that the Fe ordering may be close to that in quasicrystals. Conversely this result suggests that the strong interaction between Fe and Al (in general transition metals and Al) may be the driving force behind the formation of quasicrystals of this class.

On the other hand the interaction between Al and Ce appears to be quite normal. The Al-Ce distance is close to the sum of the atomic radii, and the short range order is basically that of the random close packing (DRP), with the repulsion between Ce atoms. Thus the short range order among Ce atoms can be described by the dilute DRP model of Ce atoms in the amorphous Al matrix. The role of Ce in this glass therefore is to stabilize the glass phase by randomness, following the mechanism suggested by the P. I. [5].

3. List of Publications.

Papers accepted or submitted for publication

* "Atomic Structure of Amorphous $Al_{90}Fe_{10-x}Ce_x$", H. -Y. Hsieh, B. H. Toby, T. Egami, Y. He , S. J. Poon and G. J. Shiflet, J. Materials Research, 5, No.12, December issue (1990).

* "Atomic Short Range Order in Amorphous $Al_{90}Fe_{10-x}Ce_x$", H. -Y. Hsieh, T. Egami, Y. He, S. J. Poon and G. J. Shiflet, J. Non-Cryst. Solids, submitted.

Papers in preparation

* "Atomic and Magnetic Structure of Ferrimagnetic Quasicrystal, $Al_{40}Ge_{25}Mn_{25}Cu_{10}$", R. Hu, T. Egami, J. J. Rhyne, A. Tsai, A. Inoue and T. Masumoto.

Abstracts published

* "Atomic Structure of Amorphous Al-Fe-Ce Determined by Pulsed Neutron Scattering", B. H. Toby, Y. He, J. D. Jorgensen, K. Volin, W. Dmowski, T. Egami, S. J. Poon, and G. J. Shiflet, Bull. Am. Phys. Soc., 34, 555 (1989).

* "Atomic Structure and Dynamics of Amorphous Al-Fe-Ce Glasses". H. -Y. Hsieh, S. Billinge, B. H. Toby, T. Egami, Y. He and S. J. Poon, Bull. Am. Phys. Soc., 35, 303 (1990).

Abstract submitted

* "Atomic and Magnetic Structure of Ferrimagnetic Al-Ge-Mn-Cu", R. Hu, T. Egami, J. J. Rhyne, submitted to the APS March Meeting.

4. List of Participating Scientific Personnel.

T. Egami	Principal Investigator
H. -Y. Hsieh	Graduate Student
R. Hu	Graduate Student
B. H. Toby	Senior Research Scientist

Degree granted

H. -Y. Hsieh, Master of Science in Engineering in Electrical Engineering, Dec., 1990.

References:

[1] L.Y. Yang, J.G. Zhao, W.S. Zhan, C.Y. Yang, Y.Q. Zhou and K.K. Fung, J. Phys. F: Met. Phys., 17, L97 (1987).
[2] A.P. Tsai, A. Inoue, T. Masumoto and N. Kataoka, Japan. J. Appl. Phys., 27, 2252 (1988).
[3] A. Inoue, K. Ohtera, A.P. Tsai and T. Masumoto, Japan. J. Appl. Phys., 27, L479 (1988).
[4] Y. He, S.J. Poon and G.J. Shiflet, Science, 214, 1640 (1988).
[5] T. Egami and Y. Waseda, J. Non-Cryst. Solids, 64, 113 (1984).
[6] A.P. Tsai, A. Inoue and T. Masumoto, Japan. J. Appl. Phys., 26, L1505 (1987).
[7] R. Hu and T. Egami, unpublished (1990).
[8] J.M. Dubois, Chr. Janot, J. Pannetier and R. Fruchart, Key Eng. Mater., 13-15, 271 (1987).

Figure Captions:

Fig. 1. Atomic pair distribution function (PDF) of icosahedral $Al_{65}Cu_{25}Fe_{10}$ determined by x-ray scattering (dashed line) and calculated from the quasicrystalline model (solid line).

Fig. 2. Neutron diffraction intensity of icosahedral $Al_{40}Ge_{25}Mn_{25}Cu_{10}$ at 10 K (solid line) and at 503 K (above the Curie temperature, dashed line).

Fig. 3. Neutron scattering intensity of the magnetic peak at 2.53 $Å^{-1}$ at various temperatures. T_c is at 194 C.

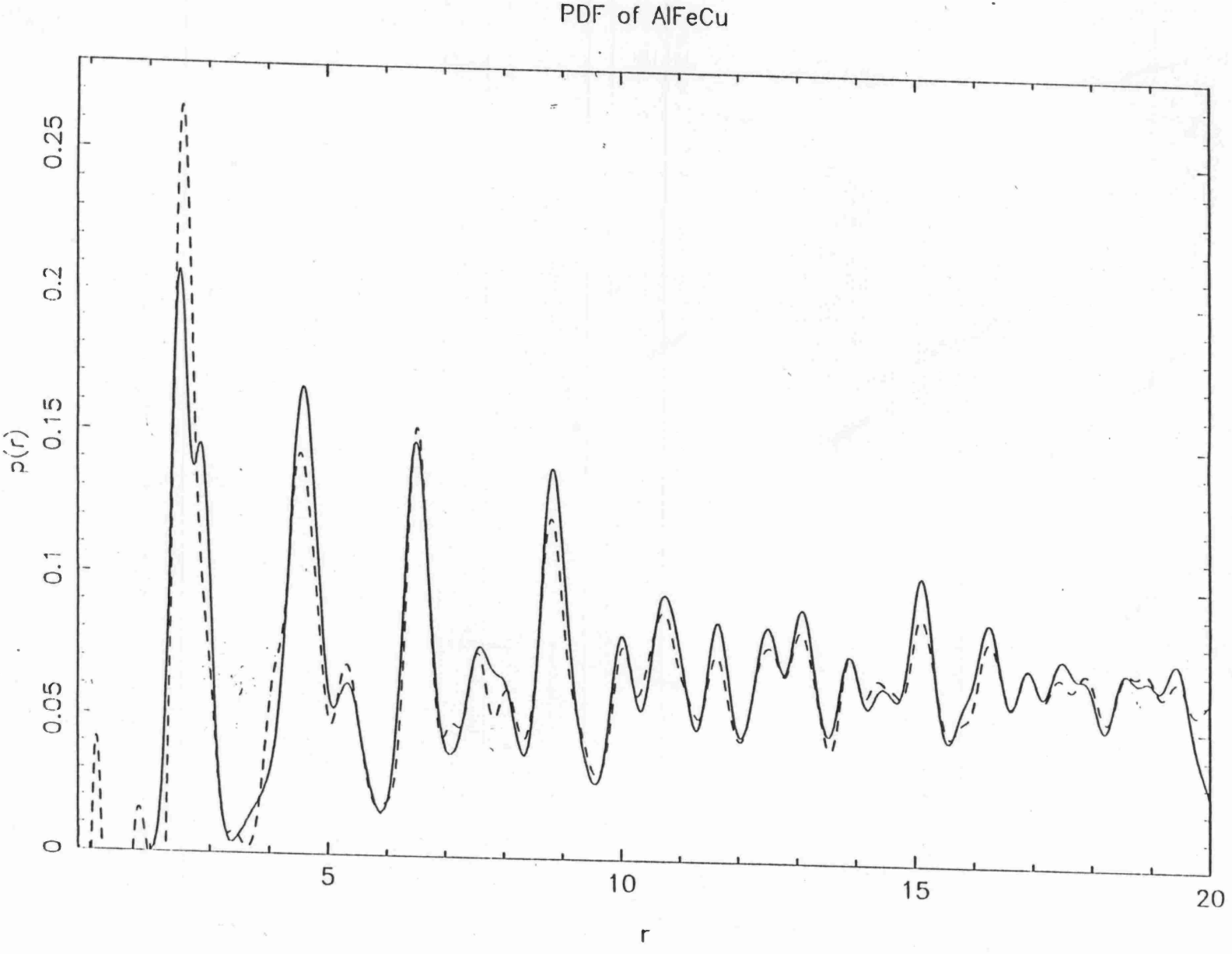

Plot of PDF of AlFeCu from X-ray data (dashed line) and calculated PDF (solid line) from the model.

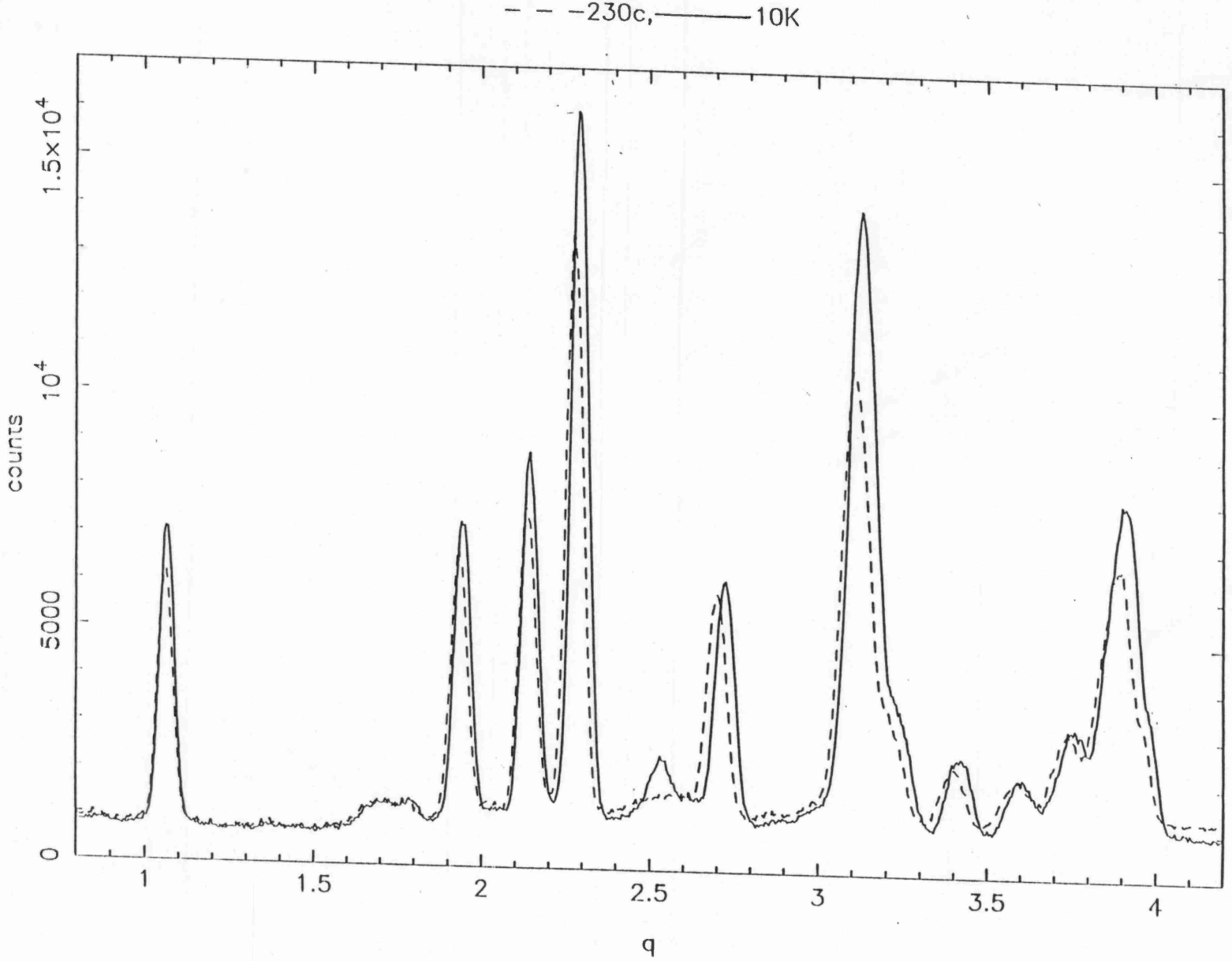

Comparison of neutron diffraction pattern of AlCuMnGe
Magnetic quasicrystal at 10K (solid) and 230 °C (dash)

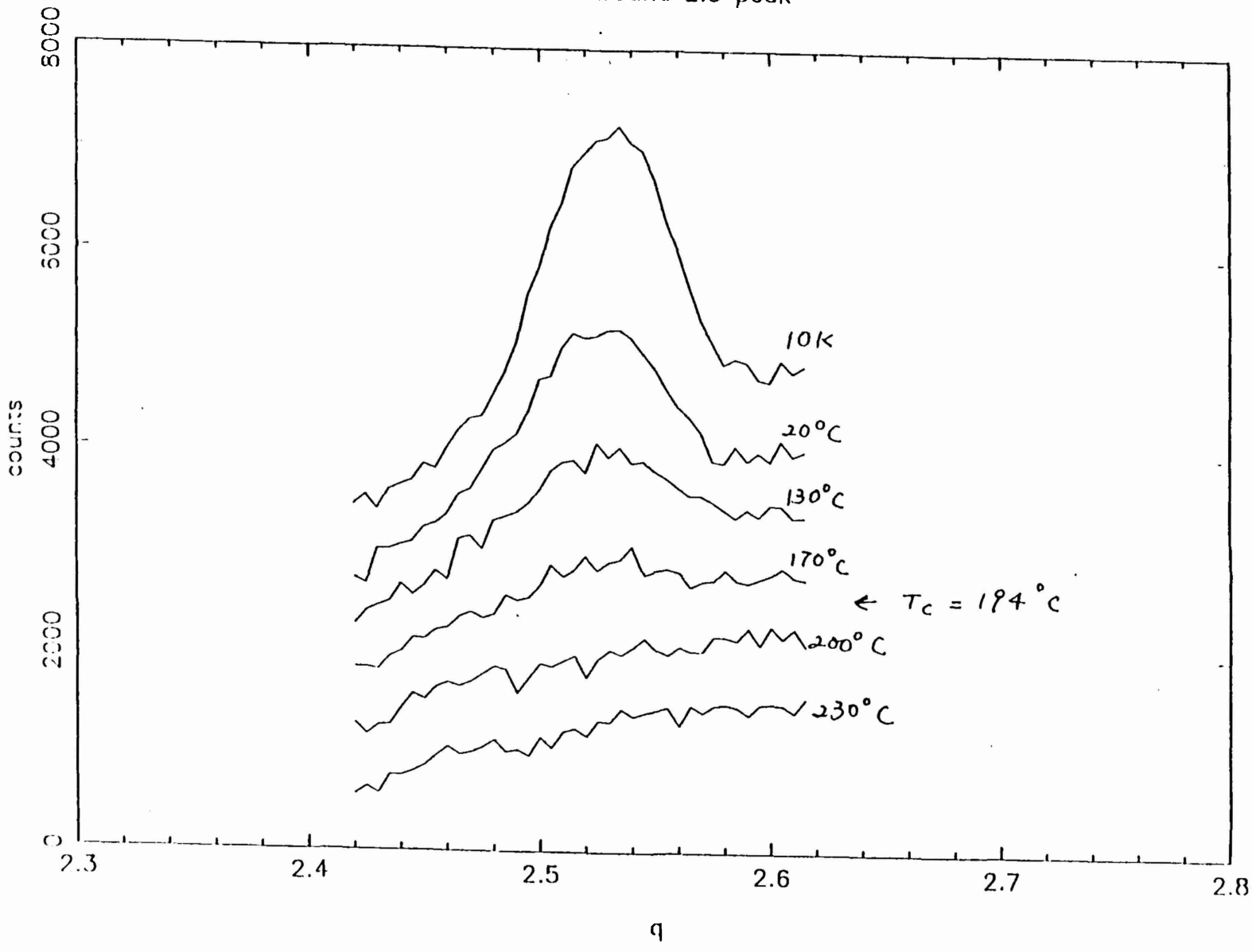

More temperature neutron diffraction runs around the magnetic peak

Atomic structure of amorphous $Al_{90}Fe_xCe_{10-x}$

H.Y. Hsieh
Department of Electrical Engineering, The University of Pennsylvania, Philadelphia, Pennsylvania 19104-6314

B. H. Toby and T. Egami
Department of Materials Science and Engineering, The University of Pennsylvania, Philadelphia, Pennsylvania 19104-6272

Y. He, S. J. Poon, and G. J. Shiflet
Department of Physics, The University of Virginia, Charlottesville, Virginia 22901

(Received 25 June 1990; accepted 20 August 1990)

The atomic structure of liquid-quenched amorphous $Al_{90}Fe_xCe_{10-x}$ ($x = 5, 7$) was studied by pulsed neutron and x-ray scattering. The atomic pair-density function determined by pulsed neutron diffraction indicates that a significant portion of Al–Fe distances is anomalously short, while some part of the Al–Al distances is anomalously long. Both neutron and x-ray scattering showed the presence of a prepeak in the structure factor. These results suggest that a strong interaction between Al and Fe modifies the structure of this glass, leading to chemical and topological short-range ordering.

I. INTRODUCTION

A group of ductile metallic glasses with aluminum up to 90 at. % were recently discovered and were found to have excellent strength per weight, or specific strength.[1,2] Examples of these glasses are Al–TM–RE (TM = Fe, Co, Ni, etc.; RE = Ce, Y, Gd, etc.), such as $Al_{87}Ni_5Y_8$, $Al_{90}Fe_5Ce_5$, and $Al_{87}Fe_{8.7}Gd_{4.3}$.[1-3] The tensile strength of $Al_{90}Fe_5Ce_5$ reaches as high as 940 MPa,[2,3] while its physical density is only 3.21 g/cm^3. Usually metallic glasses with such a high concentration of the primary element, in this case Al, cannot be formed by rapid quenching as they most often fail to satisfy the atomic size criterion for glass formability,[4] as we discuss later. The purpose of this work is to determine the origin of the glass formability through the study of their atomic structure using pulsed neutrons and synchrotron x-rays. We show that a strong interaction between Fe and Al leads to chemical and topological short-range ordering around Fe, and this contributes to the ease of formation of this glassy alloy.

II. EXPERIMENTAL RESULTS

Amorphous ribbons of $Al_{90}Fe_xCe_{10-x}$ ($x = 5, 7$) were prepared by melt-spinning in a partial helium atmosphere using a copper wheel of 20 cm in diameter, with a typical circumferential velocity of 40 m/s. In general, the dimensions were 15 μm thick, 1 to 2 mm wide, and up to several meters long. The ribbons were very flexible and could easily be bent in half without fracturing.[2] The pulsed neutron scattering experiments were carried out at the Special Environment Powder Diffraction (SEPD) spectrometer of the Intense Pulsed Neutron Source (IPNS) of the Argonne National Laboratory. The x-ray scattering measurements were performed at the X-7A beam-line of the National Synchrotron Light Source (NSLS) of the Brookhaven National Laboratory.

The chemical and geometrical atomic short-range order in amorphous materials can be determined by the neutron and x-ray scattering experiments.[5] For multicomponent amorphous systems, three formalisms (Faber and Ziman,[6] Ashcroft and Langreth,[7] and Bhatia and Thornton[8]) have been proposed to discuss the compositionally resolved structure factors to describe the chemical and geometrical order. In the following, we use the Faber–Ziman formalism. The Faber–Ziman total structure factor in the case of neutron scattering is defined as:

$$I_a^{coh}(Q) = \langle b \rangle^2 S^{FZ}(Q) + \langle b^2 \rangle - \langle b \rangle^2 \quad (1)$$

where I_a^{coh} is the coherent scattering intensity per atom, $\langle b \rangle$ is the coherent scattering length averaged over constituent atoms, $\langle b^2 \rangle$ is the square of the coherent scattering length averaged over constituent atoms, and $Q = 4\pi \sin \Theta/\lambda$, where Θ is the scattering angle and λ is the wavelength of the incident neutrons. I_a^{coh} is determined from the neutron scattering data corrected for absorption, multiple scattering, and Placzek effect.[9,10]

The Faber–Ziman total structure factor for an n-component amorphous system is expressed as the weighted sum of the partial structure factor $S_{ij}(Q)$ associated with the i-j pair correlation, where $i(j)$ is the index of i-th(j-th) components,

$$S^{FZ}(Q) = \sum_{i=1}^{n} \sum_{j=1}^{n} c_i c_j \frac{b_i b_j}{\langle b \rangle^2} S_{ij}(Q) \quad (2)$$

where c_i and b_i are concentration fraction and coherent neutron scattering length of the i-th element, and n is the number of the elements. Note that $S_{ij} = S_{ji}$. The partial

pair density function representing the *i-j* pair correlations derived by the Fourier transform of $S_{ij}(Q)$ is:

$$\rho_{ij}(r) = \rho_0 + \frac{1}{2\pi^2 r}\int_0^\infty Q[S_{ij}(Q) - 1]\sin Qr\, dQ \tag{3}$$

The total pair density function $\rho(r)$, which is the Fourier transform of $S^{FZ}(Q)$, is the weighted sum of the partial pair density functions.

$$\rho(r) = \rho_0 + \frac{1}{2\pi^2 r}\int_0^\infty Q[S^{FZ}(Q) - 1]\sin QR\, dQ$$

$$= \sum_{i=1}^{n}\sum_{j=1}^{n} C_i C_j \frac{b_i b_j}{\langle b\rangle^2}\rho_{ij}(r) \tag{4}$$

The same procedure applies to x-ray data, but x-ray data have to be corrected in addition for polarization and Compton scattering, and normalized to obtain I_a^{coh}.[11] Also, the coherent neutron scattering length b should be replaced by x-ray atomic form factor $f(Q)$ in all equations.

The neutron and x-ray scattering measurements were performed on $Al_{90}Fe_xCe_{10-x}$ samples with $x = 5, 7$. Figure 1 shows the total structure factor of $Al_{90}Fe_7Ce_3$ and $Al_{90}Fe_5Ce_5$ from the neutron scattering experiments. The total structure factor shows a double-hump main peak at about 3 $Å^{-1}$ and a small prepeak at about 1.5 $Å^{-1}$. The total structure factor from the x-ray scattering experiment shows similar features, as shown in Fig. 2. A prepeak was observed also for amorphous $Al_{90}Y_{10}$ and $Al_{87}Y_8Ni_5$.[12] Table I lists the position and area of the prepeak of the $Al_{90}Fe_5Ce_5$ and $Al_{90}Fe_7Ce_3$ samples from neutron and x-ray experiments. The position of the prepeak shifts to higher Q as the concentration of Fe increases. We may extrapolate the prepeak position to that expected for the compositions $Al_{90}Fe_{10}$ and $Al_{90}Ce_{10}$ (i.e., $Al_{90}Fe_xCe_{10-x}$ with $x = 10, 0$). The extrapolated prepeak positions for $x = 10$ and 0 are 1.58 ± 0.04 $Å^{-1}$ and 1.23 ± 0.09 $Å^{-1}$, respectively. The latter agrees with the prepeak position of amorphous $Al_{90}Y_{10}$, 1.3 $Å^{-1}$.[12]

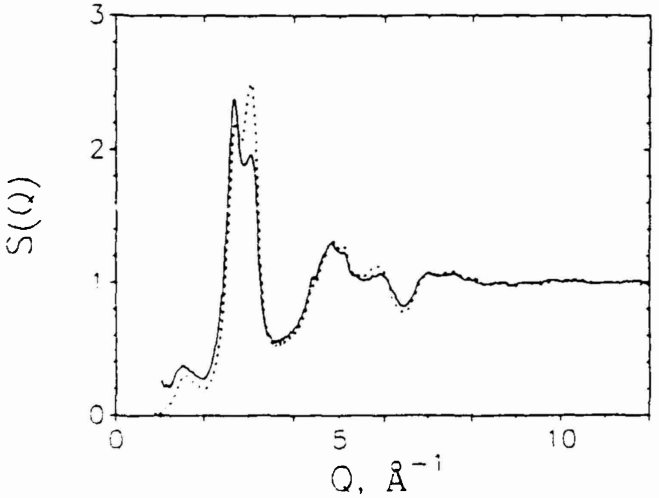

FIG. 1. Total structure factor, $S(Q)$, of amorphous $Al_{90}Fe_5Ce_5$ (solid line) and $Al_{90}Fe_7Ce_3$ (dashed line) determined by the pulsed neutron scattering experiment.

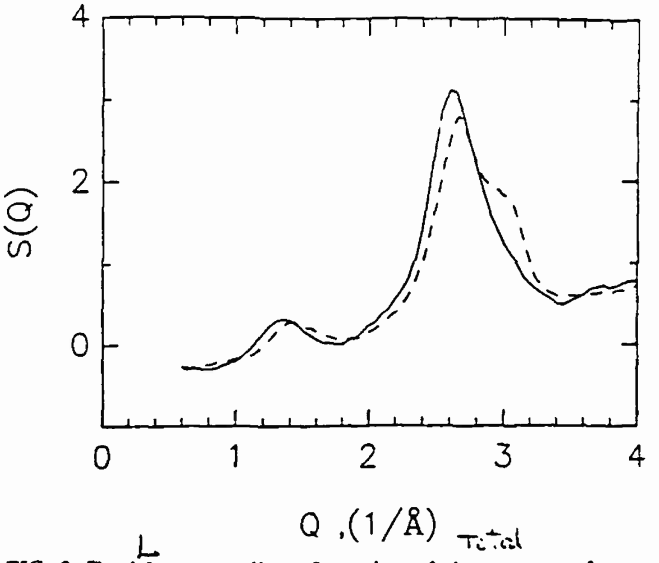

FIG. 2. Total low-to-medium Q portion of the structure factor, $S(Q)$, of $Al_{90}Fe_5Ce_5$ (solid line) and $Al_{90}Fe_7Ce_3$ (dashed line) determined by the x-ray scattering experiment.

TABLE I. First prepeak of total structure factor.

Composition	Type of experiment	Peak-position	Area
$Al_{90}Fe_5Ce_5$	Neutron	1.47	0.099
$Al_{90}Fe_7Ce_3$	Neutron	1.53	0.074
$Al_{90}Fe_5Ce_5$	X-ray	1.34	0.170
$Al_{90}Fe_7Ce_3$	X-ray	1.42	0.132

The total pair density function (PDF) of $Al_{90}Fe_5Ce_5$ and $Al_{90}Fe_7Ce_3$ from neutron experiments is shown in Fig. 3. The first peak of the total PDF apparently is not a single peak, but consists of at least three subpeaks. The first peak of the radial distribution function (RDF), $4\pi r^2\rho(r)$, of $Al_{90}Fe_7Ce_3$ was fitted by three Gaussian functions, as shown in Fig. 4. The positions and areas for the three subpeaks are listed in Table II. Also shown in Table II are the similar data for the first three subpeaks of the RDF of $Al_{90}Fe_5Ce_5$ and the difference between these two RDFs. The data for $Al_{90}Fe_5Ce_5$ are derived by fitting the first three subpeaks of the difference between the RDFs of $Al_{90}Fe_7Ce_3$ and $Al_{90}Fe_5Ce_5$, as shown in Fig. 5, and subtracting them from the data of the $Al_{90}Fe_7Ce_3$ to prevent the ambiguity in determining the subpeaks. Since the area of the first subpeak increases with the Fe concentration and Fe is the smallest atom in this alloy system, it is reasonable to assign the first subpeak to the Al–Fe correlation. The

pair density function representing the i-j pair correlations derived by the Fourier transform of $S_{ij}(Q)$ is:

$$\rho_{ij}(r) = \rho_0 + \frac{1}{2\pi^2 r}\int_0^\infty Q[S_{ij}(Q) - 1]\sin Qr\, dQ \tag{3}$$

The total pair density function $\rho(r)$, which is the Fourier transform of $S^{FZ}(Q)$, is the weighted sum of the partial pair density functions.

$$\rho(r) = \rho_0 + \frac{1}{2\pi^2 r}\int_0^\infty Q[S^{FZ}(Q) - 1]\sin QR\, dQ$$

$$= \sum_{i=1}^{n}\sum_{j=1}^{n} C_i C_j \frac{b_i b_j}{\langle b\rangle^2}\rho_{ij}(r) \tag{4}$$

The same procedure applies to x-ray data, but x-ray data have to be corrected in addition for polarization and Compton scattering, and normalized to obtain I_e^{coh}.[11] Also, the coherent neutron scattering length b should be replaced by x-ray atomic form factor $f(Q)$ in all equations.

The neutron and x-ray scattering measurements were performed on $Al_{90}Fe_xCe_{10-x}$ samples with $x = 5, 7$. Figure 1 shows the total structure factor of $Al_{90}Fe_7Ce_3$ and $Al_{90}Fe_5Ce_5$ from the neutron scattering experiments. The total structure factor shows a double-hump main peak at about 3 $Å^{-1}$ and a small prepeak at about 1.5 $Å^{-1}$. The total structure factor from the x-ray scattering experiment shows similar features, as shown in Fig. 2. A prepeak was observed also for amorphous $Al_{90}Y_{10}$ and $Al_{87}Y_8Ni_5$.[12] Table I lists the position and area of the prepeak of the $Al_{90}Fe_5Ce_5$ and $Al_{90}Fe_7Ce_3$ samples from neutron and x-ray experiments. The position of the prepeak shifts to higher Q as the concentration of Fe increases. We may extrapolate the prepeak position to that expected for the compositions $Al_{90}Fe_{10}$ and $Al_{90}Ce_{10}$ (i.e., $Al_{90}Fe_xCe_{10-x}$ with $x = 10, 0$). The extrapolated prepeak positions for $x = 10$ and 0 are 1.58 ± 0.04 $Å^{-1}$ and 1.23 ± 0.09 $Å^{-1}$, respectively. The latter agrees with the prepeak position of amorphous $Al_{90}Y_{10}$, 1.3 $Å^{-1}$.[12]

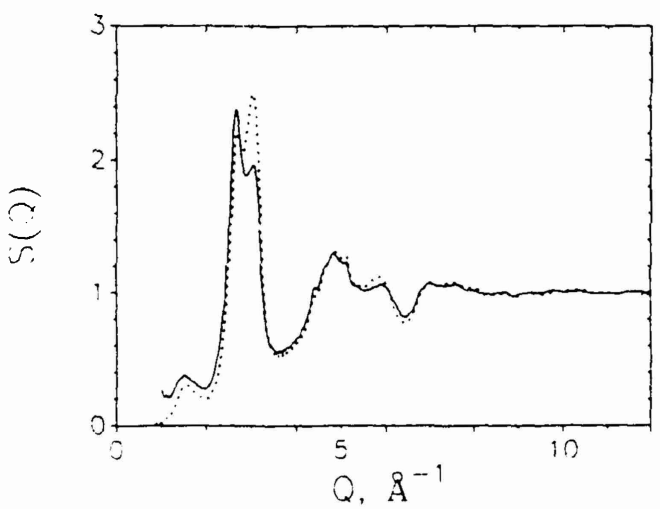

FIG. 1. Total structure factor, $S(Q)$, of amorphous $Al_{90}Fe_5Ce_5$ (solid line) and $Al_{90}Fe_7Ce_3$ (dashed line) determined by the pulsed neutron scattering experiment.

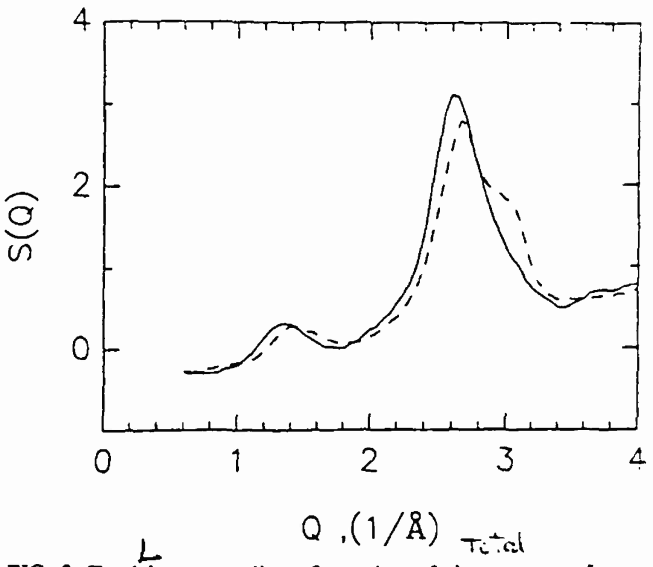

FIG. 2. Total low-to-medium Q portion of the structure factor, $S(Q)$, of $Al_{90}Fe_5Ce_5$ (solid line) and $Al_{90}Fe_7Ce_3$ (dashed line) determined by the x-ray scattering experiment.

TABLE I. First prepeak of total structure factor.

Composition	Type of experiment	Peak-position	Area
$Al_{90}Fe_5Ce_5$	Neutron	1.47	0.099
$Al_{90}Fe_7Ce_3$	Neutron	1.53	0.074
$Al_{90}Fe_5Ce_5$	X-ray	1.34	0.170
$Al_{90}Fe_7Ce_3$	X-ray	1.42	0.132

The total pair density function (PDF) of $Al_{90}Fe_5Ce_5$ and $Al_{90}Fe_7Ce_3$ from neutron experiments is shown in Fig. 3. The first peak of the total PDF apparently is not a single peak, but consists of at least three subpeaks. The first peak of the radial distribution function (RDF), $4\pi r^2\rho(r)$, of $Al_{90}Fe_7Ce_3$ was fitted by three Gaussian functions, as shown in Fig. 4. The positions and areas for the three subpeaks are listed in Table II. Also shown in Table II are the similar data for the first three subpeaks of the RDF of $Al_{90}Fe_5Ce_5$ and the difference between these two RDFs. The data for $Al_{90}Fe_5Ce_5$ are derived by fitting the first three subpeaks of the difference between the RDFs of $Al_{90}Fe_7Ce_3$ and $Al_{90}Fe_5Ce_5$, as shown in Fig. 5, and subtracting them from the data of the $Al_{90}Fe_7Ce_3$ to prevent the ambiguity in determining the subpeaks. Since the area of the first subpeak increases with the Fe concentration and Fe is the smallest atom in this alloy system, it is reasonable to assign the first subpeak to the Al–Fe correlation. The

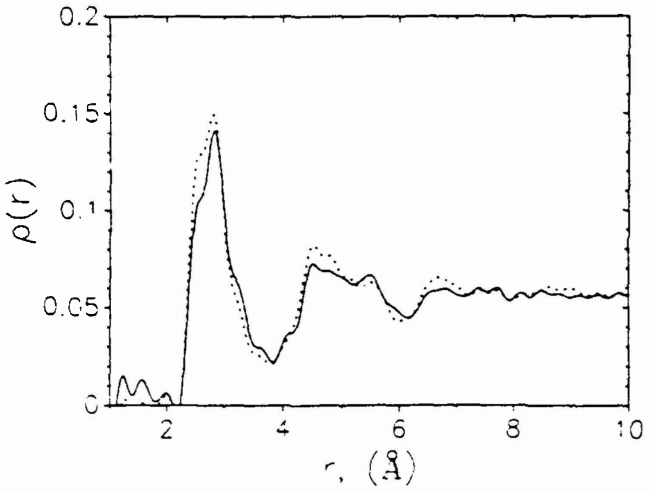

FIG. 3. Total pair density function of $Al_{90}Fe_5Ce_5$ (solid line) and $Al_{90}Fe_7Ce_3$ (dashed line) derived from the neutron scattering experiment.

Al coordination around Fe calculated from the area of the first subpeak is 6.2 and 6.3 for $Al_{90}Fe_5Ce_5$ and $Al_{90}Fe_7Ce_3$, respectively, which are identical within the margin of error, justifying the assignment of this subpeak to the Fe–Al correlation. The position of this subpeak (2.49 Å), however, is less than the sum of the atomic radii of Al (1.43 Å) and Fe (1.26 Å) by about 0.2 Å. The peak positions of the second subpeak (2.81 Å) and the third subpeak (3.25 Å) are close to the expected Al–Al distance (2.86 Å) and Al–Ce distance (3.25 Å), respectively.

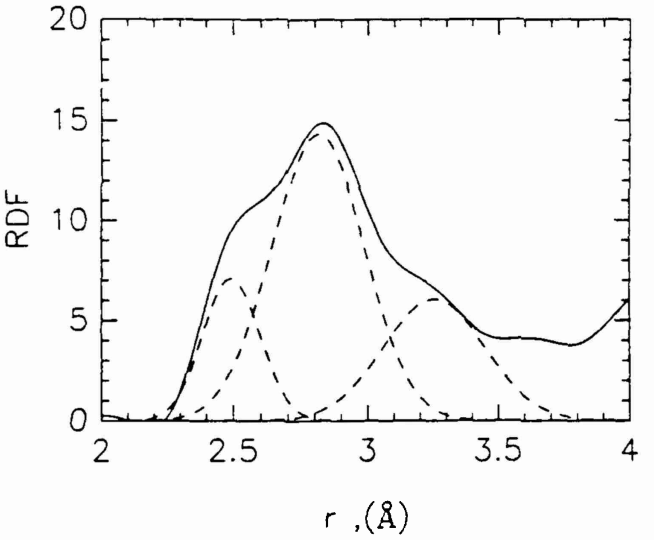

FIG. 4. The first peak of the radial distribution function of $Al_{90}Fe_7Ce_3$ fitted by three Gaussian functions (dashed lines). Areas and positions of the three Gaussian functions are listed in Table II.

TABLE II. Positions and areas of first three subpeaks of the RDF of $Al_{90}Fe_7Ce_3$ and of the difference between the RDFs of $Al_{90}Fe_7Ce_3$ and $Al_{90}Fe_5Ce_5$.

	$Al_{90}Fe_7Ce_3$		$Al_{90}Fe_7Ce_3$–$Al_{90}Fe_5Ce_5$		$Al_{90}Fe_5Ce_5$
	Position	Area	Position	Area	Area[a]
1st subpeak	2.49	1.88	2.51	0.49	1.39
2nd subpeak	2.81	6.21	2.72	0.29	5.92
3rd subpeak	3.25	2.93	3.30	−0.63	3.56

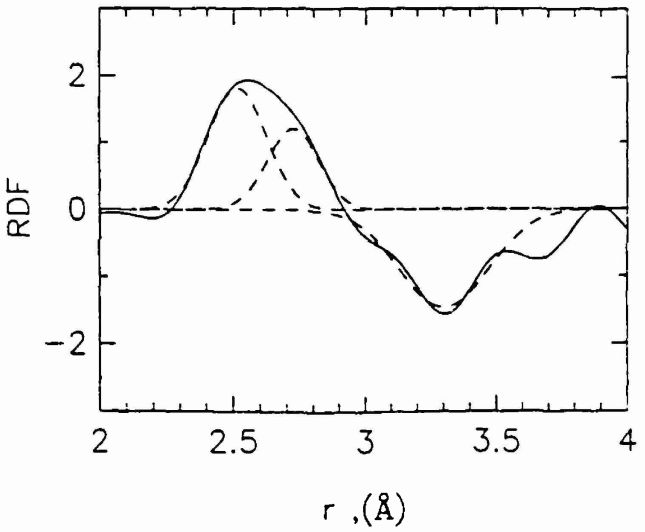

FIG. 5. Difference between the radial distribution function of $Al_{90}Fe_7Ce_3$ and the radial distribution function of $Al_{90}Fe_5Ce_5$, fitted by three Gaussian functions (dashed lines). Areas and positions of the three Gaussian functions are listed in Table II.

The average coordination number of an impurity A atom embedded in the glass of B element can be estimated accurately, within the dense random packing (DRP) model, using the principle of two-dimensional packing of the atomic surface.[13] The average coordination number is a function of the size ratio of these two atoms:

$$N_{AB} = \eta_{2D}(4(\pi/\omega_{AB}) = 4\pi(1 - \sqrt{3}/2)/\{1 - [r_A(r_A + 2r_B)]^{1/2}/(r_A + r_B)\} \quad (5)$$

where η_{2D} is the surface packing ratio, r_A and r_B are the atomic radii of the elements A and B, respectively, and ω_{AB} is the solid angle to view B atom from the central A atom. The computer simulation showed that this prediction is quite accurate over a wide range of size ratios.[14] We will refer the coordination number N_{AB} calculated from Eq. (5) as the value predicted by the DRP model. For the Al–Ce correlation such a calculation predicts a contribution of 1.08 to the area of the third peak for $Al_{90}Fe_7Ce_3$, which is much less compared to the experimental value of 2.93. Therefore, there must be contributions from other correlations. The most probable source is the Al atoms in the vicinity of Fe having long Al–Al distances. As we discussed earlier, the Fe atom has

about 6 close Al atom neighbors. If these Al atoms are evenly packed around Fe, the distance between these Al atoms should be much larger than twice the radius of the Al atom, in the neighborhood of 3.3 Å, thus contributing to the third subpeak. If we assume the remaining contribution of the area of the third subpeak comes from the elongated Al–Al distances, we can calculate the Al coordination around Al with long (3.3 Å) distances to be 2.66, which is quite reasonable for 6 contacting Al atoms. A similar estimate made for the third peak of the $Al_{90}Fe_5Ce_5$ indicates the Al coordination around Al of elongated distance is 2.27, which is slightly smaller than that of $Al_{90}Fe_7Ce_3$, but this may be due to the underestimation of the area of the third subpeak which is overlapping with the next peak.

Possible origins of the second subpeak of RDF are the Al–Al correlation and the second nearest Al neighbor around Fe. The partial pair density function $\rho_{Al,Al}(r)$ within the 1st nearest neighbor subshell will decrease when introducing Fe and Ce. Fe and Ce atoms occupy part of the nearest neighbor subshell of Al atoms and decrease the number of Al atoms contacting this Al atom. Fe also elongates the distance of Al atoms contacting it and moves some of the nearest neighbor correlation away from the first subshell at 2.8 Å. We can quantitatively evaluate the contributions by summing all the effects. For simplicity, we examined the difference of the second subpeak of the RDF of $Al_{90}Fe_5Ce_5$ and $Al_{90}Fe_7Ce_3$. There is 2% increase in the Fe number concentration and 2% decrease in the Ce number concentration when changing from $Al_{90}Fe_5Ce_5$ to $Al_{90}Fe_7Ce_3$. The calculation showed that the effects of introducing Fe and Ce are almost equal and cancel each other. Therefore the increase in the second subpeak when changing from $Al_{90}Fe_5Ce_5$ to $Al_{90}Fe_7Ce_3$ is most probably due to the second nearest neighbor of Al around Fe. With this assumption the calculated second nearest neighbor coordination of Al around Fe at a distance of approximately 2.8 Å is about 3.8. Thus there are roughly 10 Al atoms surrounding Fe within 3 Å, and about 6 of them are contacting Fe, just as in the case of crystalline compound Al_3Fe.[15]

III. DISCUSSION

A large number of alloy systems were found to form metallic glasses when they were rapidly quenched from the liquid state.[16] The question of glass formability—in other words, which factors would influence the ease of glass formation—has been discussed extensively, and a number of factors have been proposed to be the glass formability factors.[4,17,18] They include the atomic size ratio,[4,17] heat of alloy formation,[17] and valence electron concentration.[18] Among them, the atomic size ratio[4] appears to be the one with a least number of exceptions.[19] In that sense it could be identified as the most important glass formability factor. The differential atomic volume ratio was found to be inversely proportional to the minimum solute concentration necessary to form a stable glass phase by rapid quenching.[4] The approximate relationship is given by

$$C_B^{min}\left|\frac{V_A - V_B}{V_A}\right| \simeq 0.1 \qquad (6)$$

where C_B^{min} is the minimum atomic concentration of solute atoms B in the matrix of atoms A needed to form a stable glass, and V_A and V_B are the atomic volume of matrix A and solute B. For A = Al and B = Ce, C_B^{min} is 0.1; while for A = Al and B = Fe, C_B^{min} is 0.35. The size difference creates atomic level stresses which cause the topological instability of a crystalline solid solution and facilitates glass formation.[4] This equation could be generalized to ternary systems by summing the products of the minimum atomic concentration and differential atomic volume ratio of each solute element:

$$C_B^{min}\left|\frac{V_A - V_B}{V_A}\right| + C_C^{min}\left|\frac{V_A - V_C}{V_A}\right| \simeq 0.1 \qquad (7)$$

where B and C are two solute elements and A is the matrix atoms. This equation was first used successfully to describe the glass-forming range in the Co–TM–B system (TM = Ti, Zr, Hf, Cr, Mo, W, V, Nb, Ta, Mn).[20] The calculated values of the sum of the products of minimum atomic concentration and differential volume ratio for $Al_{90}Fe_5Ce_5$ and $Al_{90}Fe_7Ce_3$ are 0.067 and 0.052, respectively. These values are much less than the expected value, 0.1, indicating that the concentrations of Fe and Ce are much less than required by the equation. This is mainly due to the small atomic size difference between Al and Fe.

The shortening of the Al–Fe distance indicates a strong interaction between Al and Fe which might be the cause of high glass formability. The small number of Al coordination around Fe and the anomalously short Fe–Al distance suggests that the effective Fe radius in Al may be much smaller than the regular metallic radius, due to this interaction. We may then use Eq. (5) to define an effective size ratio according to the coordination number of Al around Fe (6.3). From the effective size ratio and the experimentally measured Al–Fe nearest neighbor distance, we can calculate the effective radius of Fe and Al and estimate the Al–Al nearest neighbor distance. The effective r_A/r_B calculated by Eq. (5) is 0.47, which implies that the effective radii of Fe and Al are 0.80 Å and 1.69 Å, respectively. Thus the distance between the adjacent Al atoms around the Fe is 3.38 Å, which is quite close to the third subpeak position of 3.25 Å. The effective size ratio also predicts the values of the sum of the products of minimum atomic concentration and differential volume ratio of the $Al_{90}Fe_5Ce_5$ and $Al_{90}Fe_7Ce_3$ systems to be

0.097 and 0.094, which is again quite close to 0.1. Thus this assumption of the reduced effective size of Fe is internally consistent, and explains very well why the unusually small concentration of the solute (Fe) atoms can stabilize the glass. The strong Al–Fe interaction and the short Al–Fe distance suggested here are consistent with the large negative deviation from volume additivity of the Al–Fe alloy in the liquid or solid state.[21] It is of interest to explore in the future whether the deviation from volume additivity is generally accompanied by unusual interatomic distances or not.

This rather drastically reduced effective size of Fe and the increased size of Al may be explained from the electronic point of view. The *d*-orbitals of Fe and the *s-p* orbitals of Al should hybridize strongly to form a delocalized *d*-band, which will be filled by the transfer of electrons from the *s-p* states as a result of the *s-p* band being pushed up in energy by the *d*-band, just as in the case of transition metal-metalloid alloys.[22] Consequently, the Fe–Al distance is reduced due to the increased Fe–Al bonding strength, while the delocalized *d*-electrons increase the Al–Al distance around Fe. Perhaps reflecting the symmetry of the *d*-orbitals, the *s-p* states of only six Al atoms hybridize with the Fe *d*-states and shorten the Fe–Al distance, while the remaining four Al atoms are only weakly in contact with Fe at the distance of 2.8 Å. A related but slightly different factor also contributes to this effect. Al has three valence electrons per atom and has a high electron density with a high Fermi level. Fe metal has 7.4 *d*-orbital electrons whose Fermi level is lower than that of Al. The difference in Fermi energy might cause a large amount of transfer of electrons from Al to Fe, but in metallic systems such a large amount of internal polarization is unstable. Instead, the effective size of Fe will be reduced to increase the Fermi level, while that of Al will be increased to balance the flow of charges.

Another point which merits further discussion is the extrapolated position of the prepeak of the total structure factor of $Al_{90}Fe_xCe_{10-x}(x = 0, 10)$. In a binary alloy system in which the minority atoms are repelling each other but more or less uniformly distributed, there will be a subpeak in the $\rho_{BB}(r)$ at a position $2r_0$ where B represents a minority element and r_0 is the average nearest neighbor distance between the minority atoms. The value of r_0 can be calculated by assuming a single-component dense random packed system with an atomic radius r_0 whose number density is equal to the number density of the minority atoms in the binary alloy system. This subpeak will be transformed to a prepeak in the partial structure factor $S_{BB}(Q)$ at $2.5\pi/r_0$ due to the law of Fourier-sine transform, the inverse relation of Eq. (3). The subpeak in the $\rho_{BB}(r)$ will emerge as a small prepeak in the total structure factor $S(Q)$ because of the small concentration of the minority atoms and thus the long distance between them. For $Al_{90}Fe_{10}$ and $Al_{90}Ce_{10}$, the prepeak position is calculated to be 1.28 $Å^{-1}$ and 1.22 $Å^{-1}$, respectively. The extrapolated position of the prepeak of $Al_{90}Ce_{10}$ is 1.23 ± 0.09 $Å^{-1}$, while the prepeak position in $Al_{90}Y_{10}$ is 1.3 $Å^{-1}$; thus both of these fit the value predicted by the dense random packing model quite nicely. This suggests that the local structure of amorphous Al–Ce(Y) might be described well by the dense random packing model, provided that the Ce–Ce potential is repulsive. For $Al_{90}Fe_{10}$, however, the extrapolated position of the prepeak (1.58 ± 0.04 $Å^{-1}$) of the structure factor is quite different from the value predicted by the DRP model (1.28 $Å^{-1}$). On the other hand, the position of the prepeak is in the close vicinity of one of the prominent diffraction peaks of quasicrystalline Al–Fe ([110001] reflection at about 1.6 $Å^{-1}$).[23] This suggests that the local structure of Al around the Fe might be similar to the quasicrystalline structure, and Fe–Al clusters may be packed with some icosahedral short-range order. In fact, a quasicrystalline icosahedral phase has been reported in rapidly cooled Al–Fe–Ce.[24] Conversely, it is possible to speculate that a strong interaction such as the one observed here may be necessary to stabilize the quasicrystalline structure.

IV. CONCLUSION

The atomic structure of $Al_{90}Fe_xCe_{10-x}$ ($x = 5, 7$) was studied by neutron and x-ray scattering measurements. Analysis of the radial distribution functions shows that the Fe atoms are surrounded by about 10 Al atoms within 3 Å, with 6 of them being in close contact with Fe. The distance between the Al–Fe pair in close contact (2.49 Å) is less than the sum of the atomic radii, suggesting a strong interaction between Al and Fe. Also, some of the Al–Al distance is elongated. The glass formability with such a high concentration of Al and the elongated Al–Al distances can be phenomenologically explained by introducing an effective atomic size ratio (0.47) between Fe and Al, which is significantly reduced from the ratio of the metallic radii of each element. The drastic departure of the effective atomic size of Fe in the matrix of Al from the regular metallic radius is most likely due to the consequence of the strong *s-d* hybridization. The analysis of the prepeak of the total structure factor indicates that Ce atoms are basically randomly distributed in the Al glass except that they are repelling each other, while a strong compositional and geometrical order exists around Fe which may be similar to the local order in quasicrystals.

ACKNOWLEDGMENTS

The authors are very grateful to D. Cox, X. Yan, W. Dmowski, R. Hu, and S. Billinge for useful sugges-

tions and for assisting with the experiments, and to Professor D. Turnbull for suggestions regarding the volume additivity. This work was supported by the Army Research Office under Contract Nos. DAAL03-87-K-0149 and DAAL03-87-K-0057. The Intense Pulsed Neutron Source is operated as a user facility by the United States Department of Energy, Division of Materials Sciences, under Contract No. W-31-109-Eng-38.

REFERENCES

[1]A. Inoue, K. Ohtera, A. P. Tsai, and T. Masumoto, Jpn. J. Appl. Phys. **27**, L479 (1988).
[2]Y. He, S. J. Poon, and G. J. Shiflet, Science **241**, 1640 (1988).
[3]G. J. Shiflet, Y. He, and S. J. Poon, J. Appl. Phys. **64**, 6863 (1988).
[4]T. Egami and Y. Waseda, J. Non-Cryst. Solids **64**, 113 (1984).
[5]K. Suzuki, in *Method of Experimental Physics: Neutron Scattering*, edited by D. L. Price and K. Sköld (Academic Press, San Diego, CA, 1987), p. 243.
[6]T. E. Faber and J. M. Ziman, Philos. Mag. **11**, 153 (1965).
[7]N.W. Ashcroft and D. C. Langreth, Phys. Rev. **159**, 500 (1967).
[8]A. B. Bhatia and D. E. Thornton, Phys. Rev. B **2**, 3004 (1970).
[9]D. L. Price, IPNS Note 19, Argonne National Laboratory, Argonne, IL.
[10]G. Placzek, Phys. Rev. **86**, 377 (1952).
[11]C. N. J. Wagner, J. Non-Cryst. Solids **31**, 1 (1978).
[12]E. Matsubara and Y. Waseda, Z. Naturforsch. **44a**, 814 (1988).
[13]T. Egami and V. Vitek, in *Amorphous Materials: Modeling of Structure and Properties*, edited by V. Vitek (TMS-AIME, Warrendale, PA, 1983), p. 127.
[14]T. Egami and S. Aur, J. Non-Cryst. Solids **89**, 60 (1987).
[15]P. J. Black, Acta Cryst. **8**, 43 and 175 (1955).
[16]C. Suryanarayana, *A Bibliography 1973–1979 for Rapidly Quenched Metals* (Plenum, New York, 1980).
[17]B. C. Giessen, *Proc. 4th Int. Conf. on Rapidly Quenched Metals*, edited by T. Masumoto and K. Suzuki (Japan Inst. Metals, Sendai, 1982), Vol. 1, p. 213.
[18]S. R. Nagel and J. Tauc, Phys. Rev. Lett. **35**, 380 (1975).
[19]S. H. Liou and C. L. Chien, Phys. Rev. B **35**, 2443 (1987).
[20]S. Ohnuma, J. Kanehira, K. Shirakawa, T. Egami, and T. Masumoto, *Proc. 4th Int. Conf. on Rapidly Quenched Metals*, edited by T. Masumoto and K. Suzuki (Japan Inst. Metals, Sendai, 1982), Vol. 2, p. 1047.
[21]D. Turnbull, Acta Metall. Mater. **38**, 243 (1990).
[22]A. P. Malozemoff, A. R. Williams, and V. L. Moruzzi, Phys. Rev. B **29**, 1620 (1984).
[23]J. M. Dubois, Chr. Janot, J. Pannetier, and R. Fruchart, Key Eng. Mater. **13–15**, 271 (1987).
[24]L.Y. Yang, J. G. Zhao, W. S. Zhan, C.Y. Yang, Y. Q. Zhou, and K. K. Fung, J. Phys. F: Met. Phys. **17**, L97 (1987).

Short Range Ordering in Amorphous $Al_{90}Fe_xCe_{10-x}$

H. Y. Hsieh

Department of Electrical Engineering, University of Pennsylvania,
Philadelphia, PA 19104-6314

T. Egami

Department of Materials Science and Engineering,
University of Pennsylvania, Philadelphia, PA 19104-6272

Y. He, S. J. Poon and G. J. Shiflet

Department of Physics, University of Virginia,
Charlottesville, VA 22901

Abstract

The atomic structure of liquid-quenched amorphous $Al_{90}Fe_xCe_{10-x}$ (x = 5, 7) was studied by diffraction method using x-rays from a synchrotron source. The diffraction data were Fourier-transformed to obtain the atomic pair-density function, and were compared to those obtained by the pulsed neutron scattering to determine the Al-Fe and Al-Ce coordination and the extent of compositional short range ordering. It was found that both Fe and Ce atoms show strong compositional short range ordering, amounting to 70 ~ 80 % of the maximum ordering possible. While Ce atoms form a dilute dense random packing substructure, the substructure of Fe atoms and the surrounding Al was found to be substantially different from the random packing, and may resemble that of quasicrystals.

1. INTRODUCTION.

A recently discovered group of Al-TM-RE (TM = Fe, Co, Ni etc.; RE = Ce, Y, Gd etc.) metallic glasses with aluminum content up to 90 atomic %, such as $Al_{90}Ni_5Y_5$, $Al_{90}Fe_5Ce_5$ and $Al_{90}Fe_5Gd_5$, show excellent strength per weight, or specific strength [1-3]. It is unusual, however, that metallic glasses with such high concentrations of the primary element, in this case Al, can be formed by rapid quenching, since they most often fail to satisfy the atomic size criterion for glass formability [4]. Our previous work [5] has shown that this unusual formability is due to the strong interaction between Fe and Al which leads to chemical and topological short range ordering (CSRO) around Fe. In this paper we will further quantify the extent of this compositional ordering by combining the results of x-ray and neutron scattering experiments.

2. DIFFRACTION EXPERIMENT.

Amorphous ribbons of: $Al_{90}Fe_xCe_{10-x}$ (x = 5, 7) were prepared by melt-spinning in a partial helium atmosphere. Typical dimensions were 15 μm thick, 1 to 2 mm wide, and up to several meters long. The x-ray scattering measurements were performed at the X-7A beam-line of the National Synchrotron Light Source (NSLS) of the Brookhaven National Laboratory. The synchrotron beam was

monochromated by a channel-cut Si (111) crystal, and the incident beam intensity was monitored by a scintillation detector counting the photons scattered by a thin poly-imid film in the beam. Since the maximum of the momentum transfer during scattering, $Q = 4\pi \sin\theta/\lambda$ where θ is the scattering angle and λ is the wave length of the x-rays, is limited by the energy of the incident x-rays, it was chosen to be high enough (24.98 keV) so that the diffraction intensity can be determined up to large values of Q and the Fourier transformation to obtain the atomic pair density function can be performed without substantial termination errors. The sample was contained in a helium environment, and the scattering study was made in the transmission geometry. The detection of scattered photons was made by a multi-wire position sensitive detector (PSD) filled with Xe/CO_2 gas. The PSD was about 10 cm long and 1 cm wide, covering about 8 degrees in the 2θ angle. We scanned the PSD with a step of 1° in 2θ from 7° to 118°, covering the diffraction vector, Q, from 0.9 to 21 $Å^{-1}$. The output from the PSD in the form of TTL pulses of which height is proportional to the position of photon detection was received by a CAMAC base multi-channel analyzer operated on-line by a micro-VAX II computer. The data from the PSD at each angle were combined to yield the scattering intensity, I(Q), which was corrected for the background due to air scattering, absorption, multiple scattering and inelastic (Compton) scattering, and normalized to obtain the total elastic scattering intensity per atom, $I_{coh}^{el}(Q)$.

3. ANALYSIS OF THE RESULTS.

In the Faber-Ziman formalism [6,7] the normalized total elastic scattering intensity is expressed in terms of the compositionally resolved partial structural factors as,

$$I_{coh}^{el}(Q) = \langle f(Q) \rangle^2 S^{FZ}(Q) + \langle f(Q)^2 \rangle - \langle f(Q) \rangle^2 \qquad (2)$$

where $f(Q)$ is the atomic scattering factor, $\langle \ldots \rangle$ denotes the compositional average, and $S^{FZ}(Q)$ is the Faber-Ziman total structure factor,

$$S^{FZ}(Q) = \sum_{i=1}^{n} \sum_{j=1}^{n} c_i c_j \frac{f_i(Q) f_j(Q)}{\langle f(Q) \rangle^2} S_{ij}(Q) \qquad (3)$$

where c_i and $f_i(Q)$ are concentration fraction and atomic scattering factor of i-th element; and n is the number of the elements, and $S_{ij}(Q)$ is the partial structure factor associated with the pair correlation between the i-th and j-th components. Note that $S_{ij} = S_{ji}$. The partial pair density function representing the i-j pair correlations derived by the Fourier transform of $S_{ij}(Q)$ is:

$$\rho_{ij}(r) = \rho_0 + \frac{1}{2\pi^2 r} \int_0^\infty Q[S_{ij}(Q) - 1] \sin Qr \, dQ \qquad (4)$$

The total pair density function $\rho(r)$ which is the Fourier transform of $S^{FZ}(Q)$ is the weighted sum of the partial pair density functions,

$$\rho(r) = \rho_0 + \frac{1}{2\pi^2 r} \int_0^\infty Q[S^{FZ}(Q) - 1] \sin Qr \, dQ = \sum_{i=1}^{n} \sum_{j=1}^{n} c_i c_j \frac{f_i(Q) f_j(Q)}{\langle f(Q) \rangle^2} \rho_{ij}(r) \qquad (5)$$

The total structure factors of $Al_{90}Fe_5Ce_5$ and $Al_{85}Fe_5Ce_{10}$ obtained from x-ray scattering experiments using a PSD are shown in Fig. 1. They show a double-hump main peak at about 2.6 $Å^{-1}$ and a small prepeak at about 1.4 $Å^{-1}$ resembling the total structure factors obtained by neutron scattering experiments [5]. A prepeak was observed also for amorphous $Al_{90}Y_{10}$ and $Al_{85}Y_8Ni_7$ [8]. Table 1 lists the position and area of the prepeak of the $Al_{90}Fe_5Ce_5$ and $Al_{85}Fe_5Ce_{10}$ samples from neutron and x-ray experiments. The prepeak area was determined by fitting a Gaussian peak with a quadratic background. The position of the prepeak shifts slightly to higher Q as the concentration of Fe increases.

The total pair density function (PDF) of $Al_{90}Fe_5Ce_5$ and $Al_{80}Fe_5Ce_{15}$ from x-ray experiments obtained by the Fourier-transformation, eq. (4), are shown in Fig. 2. The structures below 2 Å are noise due to termination and other errors. Apparently, there are at least two subpeaks at about 2.8 Å and 3.3 Å within the first peak which is consistent with the PDF obtained by the neutron experiments [5]. However, the subpeak at about 2.5 Å shown in the PDF of neutron data which correspond to the Al-Fe correlation is

not well resolved in Fig. 2. This is mainly because the relative scattering cross-section of Fe compared to the average scattering cross-section in x-ray is much less pronounced (by about a factor of two) than the relative scattering cross-section in neutron, making the contrast weaker. To obtain reliable decomposition of the first peak into three subpeaks, we used the peak positions derived from the neutron data of $Al_{90}Fe_5Ce_5$ (2.49 Å, 2.86 Å and 3.25 Å) and fitted three guassian functions to the x-ray RDF as shown in Fig. 3. The data for fitting are listed in Table 2. From this result, we calculate the Al coordination around Fe to be 7.4 and 7.5 for $Al_{90}Fe_5Ce_5$ and $Al_{90}Fe_2Ce_8$, respectively. These values are reasonably close to the neutron results on the Al coordination around Fe, namely 6.2 and 6.3 for these two compositions [5].

We also attempted to gain more information by directly comparing the x-ray and neutron results. There are three components in the $Al_{90}Fe_5Ce_5$ system, so that there are six independent pair correlation functions (Al-Al, Al-Fe, Al-Ce, Fe-Fe, Fe-Ce, Ce-Ce). This means that in principle six independent experiments with different weighting factors are needed to resolve the six pair correlation functions completely. However, the RDF is dominated by Al-Al, Al-Fe, Al-Ce correlations because of the low concentrations of Fe and Ce, and we can safely neglect the other three. Thus even from only two exeprimental results one can obtain useful information by eliminating one correlation function by suitably choosing the combining weighting factor. The RDF's from

the x-ray and neutron experiments were weighted in such a way that the dominant Al-Al contribution is eliminated upon subtraction, to obtain the Al-Fe and Al-Ce correlation. Fig 4 (a) and (b) show the difference RDF of $Al_{90}Fe_5Ce_5$ and $Al_{90}Fe_2Ce_8$ after eliminating the Al-Al correlation. The RDF's for x-ray and neutron experiments are derived from the total structure factors with the same termination (at 21 $Å^{-1}$). The RDF shows a very clear hill and valley at about 2.5 Å and 3.25 Å respectively. The new difference RDF's are dominated by the Al-Fe correlation with a positive weighting factor and by the Al-Ce correlation with a negative weighting factor. It is very reasonable to assign the first peak to the Al-Fe correlation and the first valley to Al-Ce correlation. The difference RDF' were further fitted by two Gaussian peaks to calculate the area of the first peak and valley. The data of the peak position and area are shown in Table 3. From the area, we can calculate the Al coordination around Fe and Ce. The Al coordination around Fe was found to be 4.9 and 6.4 for $Al_{90}Fe_5Ce_5$ and $Al_{90}Fe_2Ce_8$ respectively, which are close the value we reported earlier (6.2 and 6.3), and somewhat less than the values we found above. The discrepancy between these two results may stem from the ambiguity in the peak fitting. Similarly the Al coordination around Ce was found to be 14.0 for $Al_{90}Fe_5Ce_5$, and 11.0 for $Al_{90}Fe_2Ce_8$.

III. Discussion

The average coordination number of an impurity A atoms embedded in the glass of B element can be estimated accurately, within the Dense Random Packing (DRP) model, using the principle of two dimensional packing of the atomic surface [9]. The average coordination number is a function of the size ratio of these two atoms:

$$N_{AB} = \eta_{2D}(4\pi/\omega_{AB}) = 4\pi(1-\sqrt{3}/2)/[1-\{r_A(r_A+2r_B)\}^{1/2}/(r_A+r_B)] \quad (6)$$

where η_{2D} is the surface packing ratio, r_A and r_B are the atomic radii of the element A and B, respectively, and ω_{AB} is the solid angle to view B atom from the central A atom. The computer simulation showed that this prediction is quite accurate over a wide range of size ratios [10]. This equation predicts the Al coordination number around Ce to be 16.5, which is close to the value exeprimentally found for $Al_{90}Fe_5Ce_5$ (14.0), but the value for $Al_{80}Fe_5Ce_5$ (11.0) is substantially less. The discrepancy may be due to the partial oxydation of Ce which is very easily oxydized. If the actual concentration is less than the nominal concentration by 1 atomic percent, the results are in agreement with the prediction by equation (5).

The area contribution of the Al-Ce correlation to the x-ray RDF derived by difference RDF (4.17 and 2.14) is much less than the area of the third subpeak of the x-ray RDF obtained by the direct

fitting, 6.18 and 4.72 for $Al_{90}Fe_5Ce_5$ and $Al_{80}Fe_5Ce_5$, respectively. Therefore there must be contributions to the third subpeak from other correlations. The most probable source is the Al atoms in the vicinity of Fe having long Al-Al distances. As we discussed in the previous paper [5], the Fe atom has about 6 close Al atom neighbors. If these Al atoms are evenly packed around Fe, the distance between these Al atoms should be much larger than twice the radius of Al atom, in the neighborhood of 3.3 Å, thus contributing to the third subpeak. If we assume the remaining contribution of the area of the third subpeak comes from the elongated Al-Al distances, we can calculate the Al coordination around Al with long (3.3 Å) distances to be 3.3 and 3.9 for $Al_{90}Fe_5Ce_5$ and $Al_{80}Fe_5Ce_5$, respectively which is quite reasonable for 6 contacting Al atoms and further support the argument in the previous paper.

To further investigate the compositional short range ordering responsible for the prepeak of total structure factor, the area of the prepeak shown in Table 1 was compared to that of the first peak, calculated by integrating S(Q) between the two minima on the either side of the first peak. For the purpose of comparison let us consider a dilute Fe-Ce system (solute) in the amorphous Al matrix. We assume that all the Fe and Ce atoms repel each other, leading to some compositional short range ordering. Then the solute Fe and Ce atoms may form a dilute DRP structure of their own, with the average distance much larger than twice the atomic

radii due to dilution. In other words we treat the whole system as two subsystems consisting of the matrix and the solute. The first subsystem, the matrix, is composed of the DRP structure with the average scattering amplitude <b> or <f>, while the second subsystem, the solute, is made of dilute scatters of scattering length b-<b> or f-<f>, distributed with some short range order forming a DRP structure with large distances. The idea is then the prepeak in S(Q) is almost purely from the solute, or the second subsystem, while the other part of the total structure factor is mainly due to the matrix, or the first subsystem. The scattering intensity due to these two systems will be, for neutron scattering,

$$NI(Q) = \sum_{\alpha,\alpha'} b_\alpha b_{\alpha'} e^{i\vec{Q}\vec{R}_{\alpha\alpha'}} + \sum_{\alpha,\beta} b_\alpha b_\beta e^{i\vec{Q}\vec{R}_{\alpha\beta}} + \sum_{\beta,\beta'} b_\beta b_{\beta'} e^{i\vec{Q}\vec{R}_{\beta\beta'}} \quad (7)$$

$$= N_s(b_s-\langle b\rangle)^2 + N\langle b\rangle^2 S_m(Q) + (NN_s)^{1/2}\langle b\rangle(b_s-\langle b\rangle)S_x(Q)$$

where α are solute atoms and β are the matrix, N_s is the number of solute atoms, N is the total number of atoms in the system, $S_s(Q)$, $S_m(Q)$, and $S_x(Q)$ are the structure factors for the solute, the matrix, and the cross term, respectively. If both subsystems have the DRP structure, then $S_s(Q)$ and $S_m(Q)$ are connected by the scaling of the Q space,

$$S_s(Q) = S_m([\frac{N_s}{N}]^{1/3}Q). \quad (8)$$

Thus the integrated areas are related by

$$\int_P S_s(Q)\,dQ = [\frac{N_s}{N}]^{1/3}\int_{P'} S_m(Q)\,dQ, \quad (9)$$

where the integrations are made over each corresponding regions. Therefore, from equations (7) and (9), in order to compare with the area of the first peak, the integrated area of the prepeak, A_p, should be normalized by

$$A_{normalized} = A_p[\frac{(c_{Fe}+c_{Ce})\langle b\rangle}{c_{Fe}(b_{Fe}-\langle b\rangle)+c_{Ce}(b_{Ce}-\langle b\rangle)}]^2[\frac{1}{c_{Fe}+c_{Ce}}]^{4/3} \quad (10)$$

for neutrons, and by an equivalent equation for x-rays. The normalized areas are shown in Table 4. It is observed that the normalized area of the prepeak is a large fraction (70 - 80 %) of the area of the first peak, suggesting that the ordering is very extensive, and both Ce and Al are surrounded almost exclusively by Al. Since the DRP substructure represents the highest degree of ordering for the solute atoms within a glass when they try to avoid each other as much as possible, the ratio of the normalized prepeak area to the first peak area may be used as the quantitative measure of the degree of ordering. In this case, therefore, we conclude that Fe and Ce atoms achieve 70 - 80 % of the possible degree of chemical short range order.

As we discussed in the previous paper [5], the position of the prepeak is at slightly larger values of r than predicted by the DRP

model, which is about 1.25 Å^{-1}. In particular the neutron subpeaks are at higher r values, indicating that the Fe substructure, not the Ce substructure, is anomalous. This conclusion was derived also by extrapolations to $Al_{90}Fe_{10}$ and $Al_{90}Ce_{10}$, as previously discussed [5]. Together with the results on the normalized prepeak intensity discussed above, we can safely suggest that the local structure of amorphous Al-Ce might be described well by the dense random packing model, provided that the Ce-Ce potential is strongly repulsive.

However, the position of the prepeak of S(Q) extrapolated for $Al_{90}Fe_{10}$, 1.60 ± 0.04 Å^{-1}, is quite different from the value predicted by the dilute DRP model (1.28 Å^{-1}). The d-value ($2\pi/Q$) for the subpeak (4.0 Å) is much smaller than the Fe-Fe distance expected from the dilute DRP model (6.1 Å). That the Fe substructure is anomalous is not surprising in view of the strong ordering of Al atoms around Fe as we discussed previously [5]. In short, Fe atom has about 6 Al neighbors at a close distance of 2.5 Å which is considerably (by 0.2 Å) shorter than the sum of the metallic radii of Al and Fe. This is most likely because of the strong s-d hybridization between Al and Fe. This interaction must be the origin of the strong compositional ordering involving Fe. It is interesting to note that the position of the prepeak is in the close vicinity of one of the prominent diffraction peaks of quasicrystalline Al-Fe (|110001| reflection at about 1.6 Å^{-1}) [11]. This suggests that the local structure of Al around the Fe might be

similar to the quasicrystalline structure, and Fe-Al clusters may be packed with some icosahedral short range order.

IV. Conclusion

The atomic structure of $Al_{90}Fe_xCe_{10-x}$ (x = 5, 7) were studied by high-energy x-ray scattering measurements using a synchrotron sourse. By combining with the results of previous neutron scattering experiment the short range order around Fe and Ce atoms was analyzed. The results confirm the previous study [5] regarding the immediate environment of these elements, and furthermore indicate that the Fe and Ce are distributed with a strong short range order among themselves. While Ce atoms are basically randomly distributed except that they try to maximize the separation among themselves, Fe atoms strongly modify the neighboring Al atoms and result in special short range order which may resemble the icosahedral quasicrystalline order.

Acknowledgment

The authors are very grateful to B. H. Toby, D. E. Cox, X. Yan, W. Dmowski, R. Hu and S. Billinge for useful suggestions and assisting the experiments. This work was supported by the Army Research Office under contract DAAL03-87-K-0149 and DAAL03-87-K-0057, and was carried out in part at the National Synchrotron Light

Source, Brookhaven National Laboratory, which is supported by the U.S. Department of Energy, Division of Materials Sciences and Division of Chemical Sciences, and at the Intense Pulsed Neutron Source which is operated as a user facility by the U.S. Department of Energy, Division of Materials Sciences, under contract W-31-109-Eng-38.

Reference :

1. A. Inoue, K. Ohtera, A.P. Tsai, and T. Masumoto, Jpn. J. Appl. Phys., 27, L479 (1988).
2. Y. He, S.J. Poon, and G.J. Shiflet, Science, 241, 1640 (1988)
3. G.J. Shiflet, Y. He, and S.J. Poon, J. Appl. Phys., 64, 6863 (1988).
4. T. Egami and Y. Waseda, J. Non-Cryst. Solids, 64, 113 (1984).
5. H.Y. Hsieh, B.H. Toby, T. Egami, Y. He, S.J. Poon, and G.J. Shiflet, J. Mater. Res., 5, xxx (1990).
6. e.g. Y. Waseda, "The Structure of Non-Crystalline Materials -- Liquids and Amorphous Solids--" (McGraw Hill, New York, 1978).
7. T.E. Faber and J.M. Ziman, Phil. Mag., 11,153 (1965).
8. E. Matsubara and Y. Waseda, Z. Naturforsch., 44a, 814 (1988).
9. T. Egami and V. Vitek, in: "Amorphous materials: Modeling of Structure and Properties", ed. V. Vitek (TMS-AIME, Warrendale, PA, 1983) p. 127.
10. T. Egami and S. Aur, J. Non-crystalline Solids, 89, 60 (1987).
11. J.M. Dubois, Chr. Janot, J. Pannetier and R. Fruchart, Key Eng. Mater., 13-15, 271 (1987).

Figure caption:

FIG. 1. Total structure factor, S(Q), of amorphous $Al_{90}Fe_5Ce_5$ (solid line) and $Al_{90}Fe_5Ce_5$ (dashed line) determined by x-ray scattering experiments.

FIG. 2. Total pair density function of $Al_{90}Fe_5Ce_5$ (solid line) and $Al_{90}Fe_5Ce_5$ (dashed line) derived from the x-ray scattering experiments.

FIG. 3. The first peak of RDF of $Al_{90}Fe_5Ce_5$ fitted by three Gaussian subpeaks at 2.49 Å, 2.81 Å and 3.25 Å.

FIG. 4. (a) Difference RDF of $Al_{90}Fe_5Ce_5$ between x-ray and neutron experiments with the Al-Al correlation eleminated, (b) same for $Al_{90}Fe_5Ce_5$.

Table 1. First prepeak of the total structure factor:

Composition	Type of experiment	Peak-position ($Å^{-1}$)	Area ($Å^{-1}$)
$Al_{85}Fe_5Ce_{10}$	neutron	1.53	0.051
$Al_{90}Fe_5Ce_5$	neutron	1.56	0.067
$Al_{85}Fe_5Ce_{10}$	x-ray	1.35	0.174
$Al_{90}Fe_5Ce_5$	x-ray	1.38	0.149

Table 2. Positions and areas of first three subpeaks of the RDF of $Al_{85}Fe_5Ce_{10}$ and $Al_{90}Fe_5Ce_5$ determined by x-ray scattering experiment.

	$Al_{85}Fe_5Ce_{10}$		$Al_{90}Fe_5Ce_5$	
	Position*	Area ($Å^{-1}$)	Position*	Area ($Å^{-1}$)
1st subpeak	2.49	1.10	2.49	1.53
2nd subpeak	2.81	4.57	2.81	5.21
3rd subpeak	3.25	6.18	3.25	4.72

* The position is derived from the neutron experiments [5].

Table 3. The peak position and the area of the subpeak of the weighted difference RDF from x-ray and neutron experiments

Composition	Position (1st subpeak)	Area ($Å^{-1}$)	Position (2nd peak)	Area ($Å^{-1}$)
$Al_{90}Fe_5Ce_5$	2.43	0.464	3.26	-5.26
$Al_{85}Fe_5Ce_{10}$	2.52	0.847	3.27	-2.49

Table 4. The area of the prepeak normalized by equation (10) and the area of the first main peak of the structure factor, S(Q).

Composition	Type of measurement	Prepeak Area A_{norm} ($Å^{-1}$)	First Peak Area A_1 ($Å^{-1}$)
$Al_{90}Fe_5Ce_5$	x-ray	1.39	1.84
$Al_{85}Fe_5Ce_{10}$	x-ray	1.82	1.80
$Al_{85}Fe_5Ce_{10}$	neutron	1.40	1.93
$Al_{90}Fe_5Ce_5$	neutron	1.26	2.01

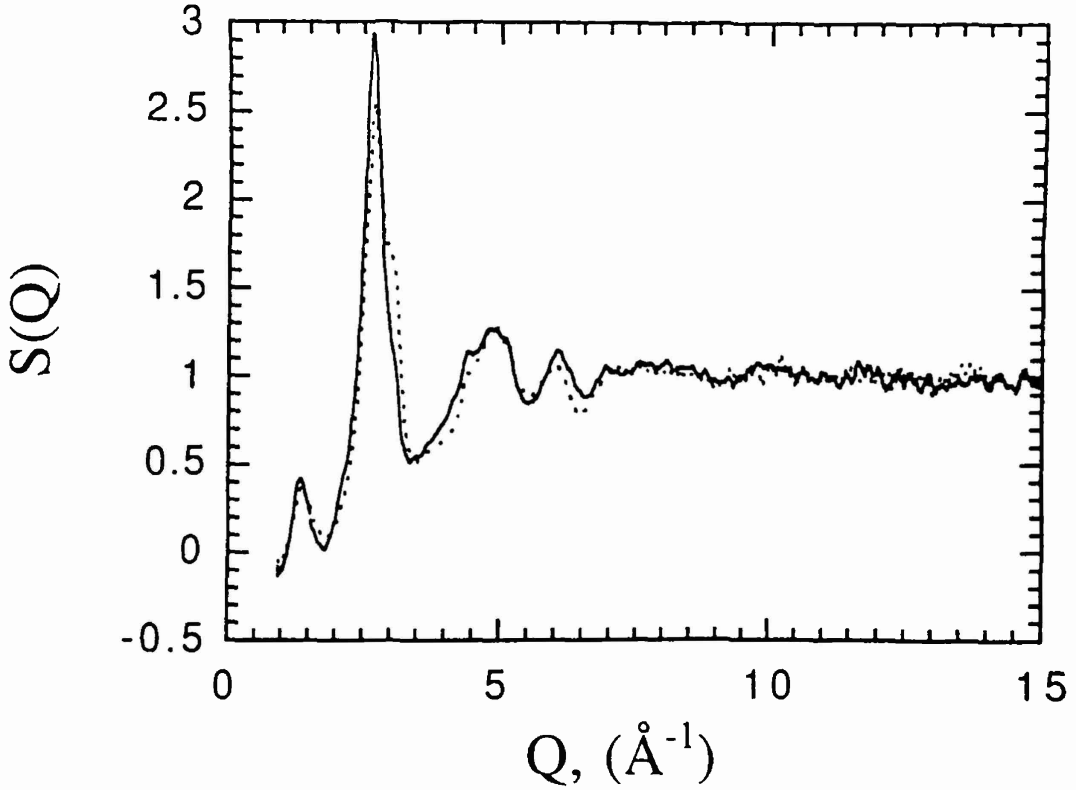
S(Q)
3
2.5
2
1.5
1
0.5
0
-0.5
0
5
10
15
Q, (Å-1)

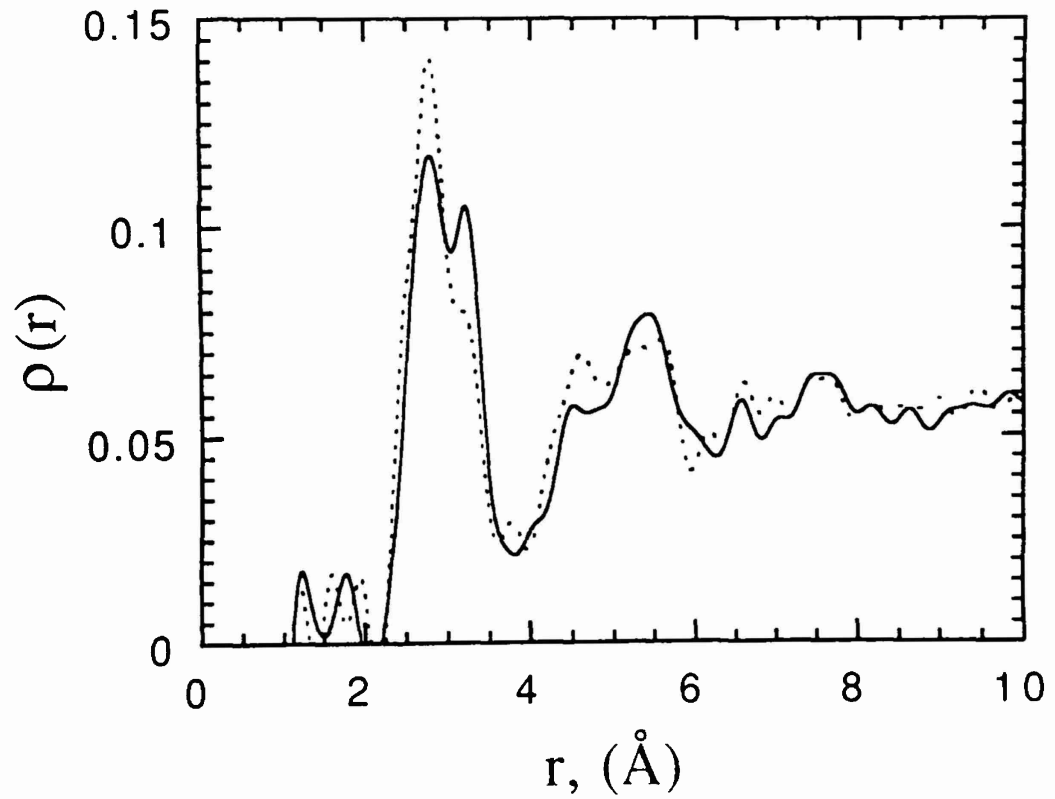
ρ(r)
0.15
0.1
0.05
0
0
2
4
6
8
10
r, (Å)

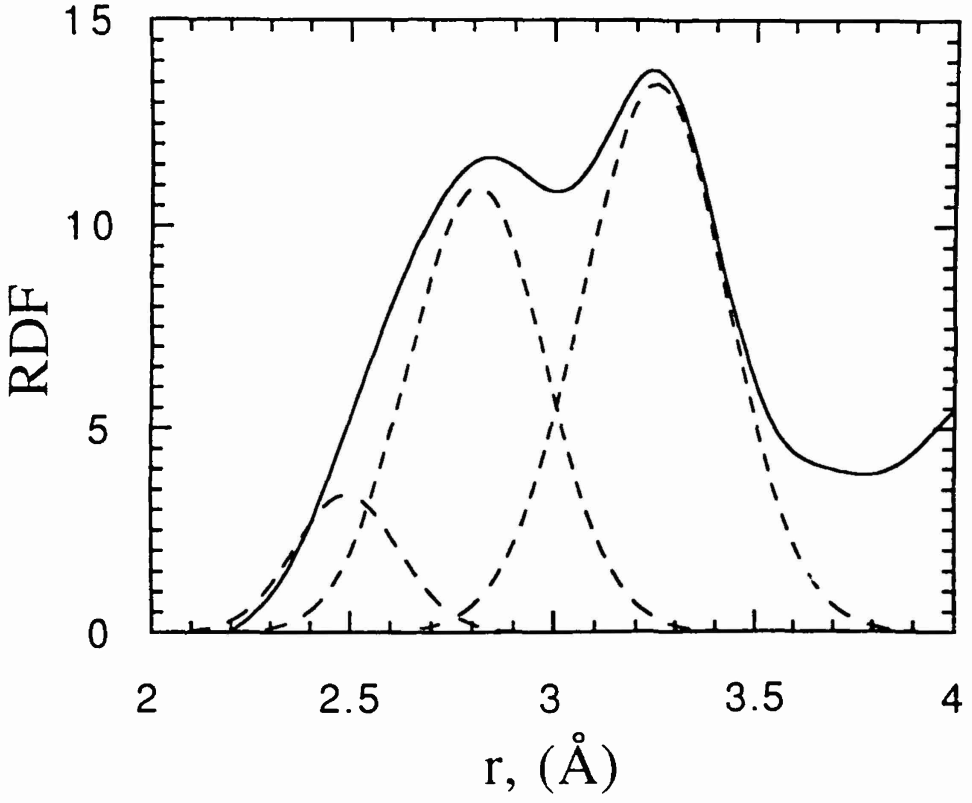
15
10
5
0
RDF
2
2.5
3
3.5
4
r, (Å)

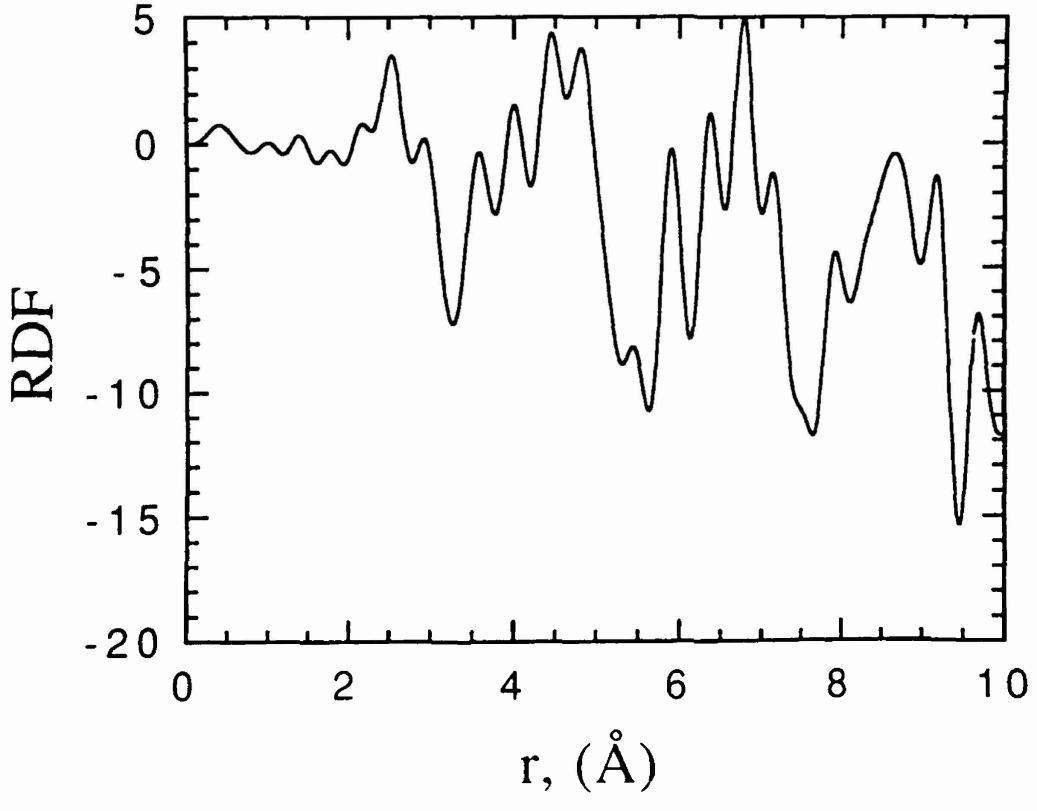
5
0
-5
-10
-15
-20
RDF
0
2
4
6
8
10
r, (Å)

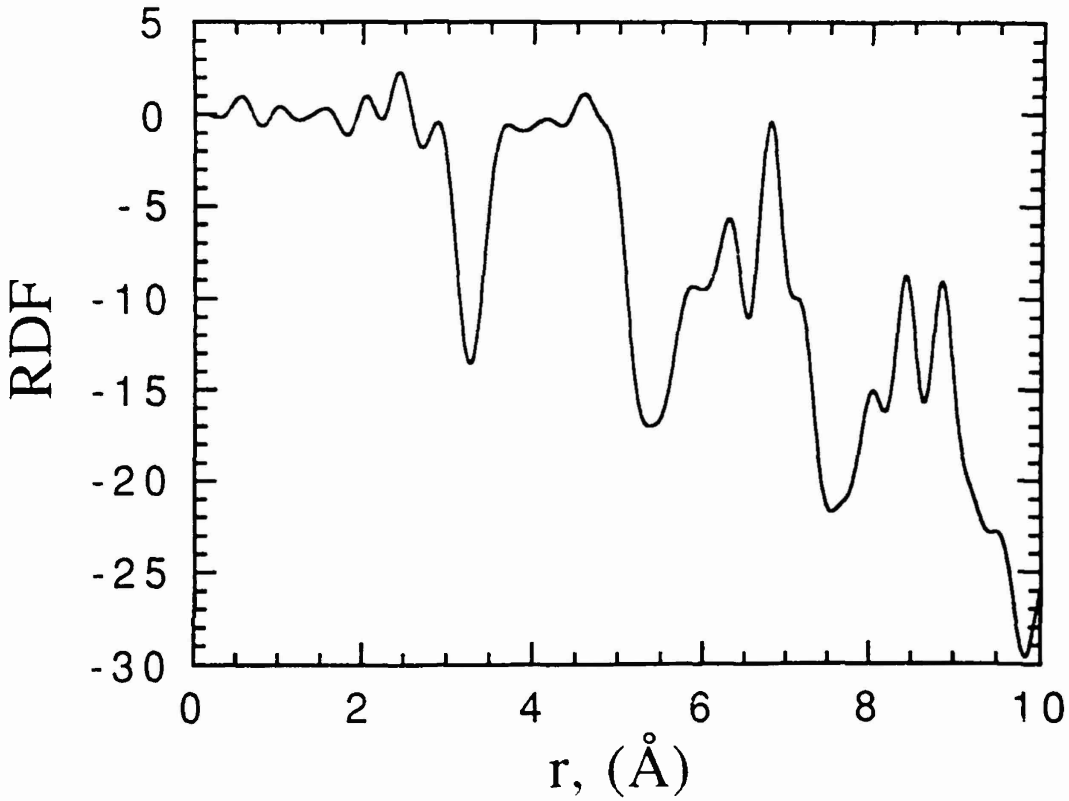
RDF
5
0
-5
-10
-15
-20
-25
-30
0
2
4
6
8
10
r, (Å)